Corrosion Behavior of the Nickel/nickel Interface During the Copper Sacrificial Layer Releasing Process in Micro-Electroforming

Lili Wang
    China Academy of Engineering Physics Institute of Machinery Manufacturing Technology

Minheng Ye
    China Academy of Engineering Physics Institute of Machinery Manufacturing Technology

Yingying Wang
    China Academy of Engineering Physics Institute of Machinery Manufacturing Technology

Dong Tian
    China Academy of Engineering Physics Institute of Machinery Manufacturing Technology

zuoyan Ye (✉ yebonpu@126.com)
    China Academy of Engineering Physics Institute of Machinery Manufacturing Technology

Chao Wang
    China Academy of Engineering Physics Institute of Machinery Manufacturing Technology

---

Abstract

The corrosion behavior of the Ni/Ni interface during the Cu sacrificial layer releasing process in micro-electroforming has been investigated. The XPS and SEM results reveal that the pre-existing passive layer and interfacial defects exist on the Ni/Ni interface. Compared with Ni base, the interface is prone to be attacked. Pitting corrosion occurs along interface boundary, which contains three main processes, pit initiation, pit growth and pits fusion, leading to a commensurate reduction in interfacial adhesion strength and ultimately structural integrity. The combination of the substrate modification and heat post treatment is an effective solution to avoid the localized corrosion. We believe that both the surface activation and thermally induced diffusion have worked.

1. Introduction

With high manufacturing accuracy, low cost and mass production capacity, electroforming technologies, especially base on mask molding and layered fabrication, have become an irreplaceable method to manufacture complex 3D metal micro devices in MEMS, such as micro gear, micro inertial switch, micro actuator, which are expected to be applied in microwave communication, aerospace, weapon equipment and other fields [1–5].

To electroform a multilayered microstructure successfully, the adhesion between adjacent layers is critical, which significantly affects the mechanical performance, reliability and serve time of the micro device [6–7]. Weak interface bonding can even lead to the warpage or delamination of electrodeposited layers and finally result in the fabrication failure. At present, many methods have been adopted to improve the adhesion strength, including surface activation prior to plating [8], regulating electrodeposit current density [9] and ultrasound-assisted electrodeposit method [10]. However, post-processes, photoresist removal and sacrificial layer release, also have great effects on the interfacial bonding strength, which are rarely investigated.

The Sacrificial-Layer technique is essential to the layered mask molding based fabrication of high aspect ratio structures and especially movable suspension parts in MEMS devices. The metal Cu, Zn, Ti and SU-8 photoresist are usually utilized as sacrificial layer materials. The etchants to remove sacrificial layer are inorganic acid, e.g. hydrochloric acid, and oxidizing agents, including ferric chloride, chlorite, peroxide and persulfate [11–15]. Inevitably, these etchants can also corrode the structural metals (e.g. Ni, NiFe) with slow etching rate. Du et al. [16] dissolved the thick SU-8 sacrificial layers in the boiling inorganic acid solution and the Ni structural layers were etched simultaneously resulting in the dimension errors between design and the actual dimension of the microstructure. The effective etching solution, based on an additive complex in the ammonia liquor with the assistance of violent oxidant, was proposed by Wu et al. [17] to selectively etch thick (>100μm) sacrificial Cu laminations with the etching rate of 156μm/h, while Ni structure layers were also dissolved at approximately 0.1μm/h. A two-component, ammonium hydroxide and chlorite, was the another effective stripper designed by Zhang et al. [18] to remove Cu as fast as 460μm/h. Although this etchant had good compatibility with Ni with the corrosion rate of only

0.01μm/h, some pits were observed to form on the Ni structure layers. In contrast to uniform corrosion, whose rate will normally be predictable, pitting corrosion tends to proceed at an unexpected and high rate of localized metal dissolution. Obviously, pitting corrosion on Ni structure layers is unacceptable to microstructures. Just as many literatures have proved [19–21], the presence of aggressive species, such as haloid ion, sulfate, and metallurgical heterogeneity, such as inclusions, dislocations, interfaces, and grain boundaries, facilitate the localized corrosion on a metal. For a multi-layered Ni microstructure, the Ni/Ni interfaces are the main metallurgical heterogeneities and supposed to be attacked preferentially in the etching process of the sacrificial layer compared with the Ni base. Especially, after long-time releasing of the ultra-thick (>700μm) sacrificial layer, the localized corrosion of the interfaces is supposed to be severe and will badly decrease the interfacial bonding strength. Hence it is essential to study the corrosion behavior of the Ni/Ni interface, which had yet to be conducted in previous literatures.

By sharing this insight, we report the corrosion behavior of the Ni/Ni interface during the wet-etching process of the ultra-thick (>700μm) Cu sacrificial layer in ferric chloride solution. Six kinds of Ni/Ni interface were obtained by altering the pre/post-treatments, including degreasing, in-situ anodic treatment, pickling, repassivation and heat-treatment. The activity and chemical characteristic of the pre-treated Ni substrates were explored by the OCP and XPS tests. The microstructures of as-prepared Ni/Ni interfaces were investigated by scanning electron microscopy. Moreover, the corrosion type and depth of the Ni/Ni interfaces were tested by the 3D microscope with ultra-depth of field. Based on the evolution of corrosion damage, the corrosion behavior of the Ni/Ni interface was studied and the corrosion mechanism was depicted, providing guidance for improving the corrosion resistance performance and interface bonding energy.

2. Material And Methods

2.1 Preparation of the Ni/Ni interface

In this study, a 2mm-thick T2 copper substrate (purity ≥ 99.9%) with an exposed area of 30mm×30 mm was chosen as the substrate for the multilayered Cu/Ni structure. The Cu sacrificial layer was prepared in the standard copper plating electrolyte composed of $CuSO_4•5H_2O$ and H_2SO_4 solution with additives at a current density of 3A/ dm^2. The Ni structure layer was conducted under pulse current conditions at 50°C in a nickel sulphamate bath, which contained 350g/L $Ni(NH_2SO_3)_2$, 10g/L $NiCl_2$, 35g/L H_3BO_3 and 0.2g/L wetting agent, with the pH value of 4.0. The average current density, frequency and duty ratio of the applied currents were 3.75A/dm^2, 1000Hz, 20%, respectively. After plating for five hours, about 200μm-thick Ni layer was obtained. Subsequently, it was grinded and polished to a relatively smooth surface which would be the substrate for the next Ni layer. As shown in Fig. 1, multilayer nickel structure was fabricated simulating MEMS electroforming process.

Prior to electrodepositing the latter Ni layer, five kinds of pretreatments were used to remove residual impurities and/or remaining oxides from the former Ni substrate. The detailed description of the pretreatment of Ni substrate was given as follows. As a control group forming the standard of

comparison in this research, the Substrate-▢ was not pretreated. The Substrate-▢ was electrolytically degreased at 70°C during 5 min in a bath of alkaline solution under constant current condition ($4A/dm^2$). The Substrate-▢ was degreased as the second one and then electrolyzed in the nickel sulphamate bath using as an anode at a current density of $2A/dm^2$ for 5min. The Substrate-▢ was also degreased firstly and pickled in a hydrochloric acid solution (50%v/v) for 10min. To further study the effect of surface nickel oxide on interfacial property, artificially thicker oxidized layer was created by oxidizing the Substrate-▢ in concentrated nitric acid.

Pre-conditioned Ni substrates were rinsed by deionized water and transferred without delay to the nickel sulphamate bath whereafter electrodepositing started severally under the same plating conditions as the first Ni layer. Five interfaces formed concomitantly and were designated as Interface-▢, Interface-▢, Interface-▢, Interface-▢ and Interface-▢, successively. A post-heat-treatment of the Interface-▢ was carried out at 450°C with holding time of six hours. And the reborn interface was denominated as Interface-▢.

2.2 Specimen characterization

For testing the efficacy of the pretreatments, open circuit potential (OCP) of the pretreated nickel substrate in a 5% Na_2SO_3 solution was performed in a standard three-electrode cell consisting of a working electrode, a saturated Ag/AgCl reference electrode and a Pt foil counter electrode. All the measurements conducted with a PGSTAT302N electrochemical workstation (Metrohm Corporation) at 25°C last until a change of less than 10^{-6}V/s. Na_2SO_3 as a reducing agent was employed to minimize the oxygen content in the solution, avoiding the repassivation of the preconditioning nickel substrates.

The surface characteristics of the pre-treated Ni substrates were measured by X-ray photoelectron spectroscopy (XPS, AXIS-Ultra) using monochromatic Al Kα radiation with 1486.71 eV operating at 16 kV. To compensate for surface charge effects, binding energies were calibrated using the C 1s hydrocarbon peak at 284.80 eV.

The cross-sections of the multi-layered structure were mildly wiped by a mixed solution of 38mL concentrated HNO_3, 100mL concentrated CH_3COOH and 10mL H_2O for three seconds, which was a standard metallographic etchant for electrodeposited Ni. Then the cross-sectional metallographic micrographs and interfacial microstructures were investigated by Optical microscopy (OM, Zeiss Axio Observer A1m) and scanning electron microscopy (SEM, Zeiss Ultra 55).

2.3 Chemical etching of sacrificial layer

Ferric chloride solution is an extensively used etchant for Cu in the Printed Circuit Board and surface finishing industry. With a high etching rate and good selectivity, it was chosen to release ultra-thick copper sacrificial layer (> 700μm). The solution was prepared by mixing 30g $FeCl_3·6H_2O$, 2mL HCl and 200 mL H_2O. The as-prepared Cu/Ni multi-layered structure was incised into 5mm×5mm×2mm blocks by a cutting machine. After polishing, the block was put into a string bag and suspended in the etchant

solution for 120min. The etching images and depth profile analyses were performed using a LH-WN-YH 3D microscope with ultra-depth of field manufactured by Chengdu Liyang Precision Machinery Co., Ltd.

3. Results And Discussion

3.1 Activity and surface characteristics of the pretreated substrates

After mechanically grinding and polishing, dust, organic pollutants and passive oxide layer remained on the surface of Ni substrate. Without any treatment, these impurities would act as barriers against the bonding between Ni substrate and Ni electrodepositing layer which would be the imperfection of the interface resulting in poor adhesion strength and corrosion resistance [22-23]. To improve the interfacial bonding strength, surface activation prior to plating was performed. The open circuit potentials (OCP) before and after pretreatments were measured to indicate the degree of electrode activation since the more negative the potential, the more active the substrate. The OCP results and corresponding substrates were listed in Table 1.The stable potential of the untreated Substrate-Ⅰwas -0.428V (vs. Ag/AgCl). Deoiling treatment of the Substrate-Ⅱand in-situ anodic treatment of the Substrate-Ⅲ resulted in the potential negative shift slightly. After two-step pretreatments, degreasing and pickling, the potential of the Substrate-Ⅳ was -0.528V (vs. Ag/AgCl) which was the most negative among the five substrates. Conversely, because of the repassivation in concentrated nitric acid, the OCP of the Substrate-Ⅴ was -0.331V (vs. Ag/AgCl) and even more positive than that of the untreated one.

Table 1 The OCP results of the pretreated Ni substrate

Substrate	Substrate-Ⅰ	Substrate-Ⅱ	Substrate-Ⅲ	Substrate-Ⅳ	Substrate-Ⅴ
Pretreatment	Untreated	Degreasing	Degreasing+ Anodic Treatment	Degreasing+ Pickling	Degreasing+ Repassivation
OCP/V vs. Ag/AgCl	-0.428	-0.453	-0.470	-0.528	-0.331

To examine the surface characteristics of the substrates, XPS measurements were performed. After pretreatments, the substrates were rinsed by deionized water and tested as soon as possible. The changes of the oxide layer on the substrate induced by the pretreatments were clearly manifested by the $Ni2p_{3/2}$ spectra (Figure 2(a)-(e)). Two main peaks at 852.5 eV and 855.7 eV were originated from metallic Ni (Ni^0) and $Ni(OH)_2$ respectively. The broad shake-up peak at about 860.9 eV was the satellite of the main peaks, which could be attributed to the multi-electron excitation. [24-25] The proportion of the metallic Ni (Ni^0 %) on the substrate was figured out by the peak area ratio of the Ni^0-related peak and $Ni(OH)_2$-related peak. The Ni^0 % of the Substrate-Ⅳ (48%) was higher than that of the Substrate-Ⅱ(18%) and as high as about five times of the Substrate-Ⅰ(10%) and Substrate-Ⅲ(9%). The Ni^0 % of the Substrate-Ⅴ nearly became zero. On the whole, both the OCP and the XPS results indicated that the Substrate-Ⅳ was

the most activated while the Substrate-Ⅰ was totally passivated. Obviously, pickling is an effective method to improve the proportion of the metallic atoms on the substrate by the surface activation mechanism, in favor of the formation of the tight Ni electrodeposits.

On the whole, both the OCP and the XPS results indicated that the Substrate-Ⅲ was the most activated while the Substrate-Ⅰ was the least activated. After Ni layer was electroformed on the pretreated substrate, the impurities on the substrate would be the inclusions and imperfections of the Ni/Ni interface.

3.2 Microstructural characterization of the Ni/Ni interface

To clearly observe the cross-sectional characteristics of the as-prepared multilayered Ni structures, the sections were polished and etched by nitric acid-acetic acid mixed solution. As shown in Figure 3, the boundary lines, also called interfaces between two Ni layers, were obvious and marked by Roman numerals in order. For more detailed interfacial microstructures, SEM micrographs of the Ni/Ni interfaces were taken and presented in Figure 4. Compared with Ni base, the interface always contains imperfections, including dislocations where the atoms are mismatched between adjacent lattices, each with a different orientation, and cavities where organic/oxide residua on the substrate hinder the formation of the electrodeposited layer. The widths of the Interface-Ⅰ, Interface-Ⅱand Interface-Ⅲ are all about 100nm. But the cavity size on the interface goes down and cavity number decreases in turn. Interface-Ⅲ has the width of approximately 50nm with only few tiny cavities. The width of the Interface-Ⅰis as long as 250nm. Undoubtedly, the number of the interface defects is proportional to the width of the interface and the size and number of the cavities on the interface. There are reasons to believe that the imperfections on the Interface-Ⅲ are the least while the imperfections on the Interface-Ⅰ are the most.

Besides, it can be inferred from XPS and SEM results that the superficial state of the substrate is critical to the interfacial property. As the substrates are cleaned and activated, the interface becomes thinner and the cavities on the interface becomes less. Actually, maintaining an absolutely activated nickel substrate during the time required to transfer the component from the activated process to the plating solution seems to be impractical which can also be proved by the XPS results. Hence, although the Substrate-Ⅲ was activated in hydrochloric acid solution for a long time, there were imperfections on the Interface-Ⅲ. In order to further minimize interface defects, a post-heat-treatment was adopted. The specimen containing the Interface-Ⅲ was held at the annealing temperature of 450°C(below recrystallization temperature of Ni metal) for 6h. The microstructure of the reborn Interface-Ⅲ was characterized by SEM, as shown in the Figure 4(f). The width of the Interface-Ⅲ was only 20nm and no obvious cavities appeared. Owing to the thermally induced diffusion of Ni and O atoms at the interface, the dislocations and defects density decreased which could effectively improve the interfacial property in accordance with previous studies [26-27].

3.3 Corrosion behavior and corrosion mechanism of the Ni/Ni interface

The as-prepared laminated Ni structure with ultra-thick Cu sacrificial layer was selectively released by the ferric chloride solution. The specific process was described in Experimental section. Optical micrographs

of etching faces and corresponding corrosion damage profiles of the laminated structure were presented in Figure 5. The passivation of nickel by the growth of Ni2+ anodic oxides on the surface in both acidic and alkaline environments was well-documented [28-29]. The passive film was dense and stable, locking access of the environment to the metal. Therefore compared with passivated Ni layer, Cu layer dissolve more easily in ferric chloride solution. Not surprisingly, a distinguished difference in the etching rates of Cu sacrificial layer and Ni electroformed layer could be seen from Figure 5(b) and 5(e), with about 700μm drop at Cu/Ni interface. The etching rate of Cu was approximately 350μm/h. As seen in Figure 4(c), Ni/Ni interfaces were more susceptible to be corroded than the nickel base. After etching in the ferric chloride solution for 120min, deep etching trenches were formed along the Interface-I, Interface-⬚ and Interface-⬚, with the penetration depths of about 30μm, 28μm and 20μm respectively. Even, this kind of preferential corrosion led to the debonding of Interface-⬚ (see Figure 4(e)). Differently, some shallow corrosion pits (pointed by the red arrows), with diameters of 7~10μm, were formed instead of corrosion trench on the Interface-⬚,as revealed by the enlarged image Figure 5(f). From Figure 5(g) and (i), it can be seen that, even etching for 140min, the Interface-⬚ remained almost intact and kept uniform corrosion along with the nickel base. It fully proved that the post-heat-treatment could remarkably improve the resistance to localized corrosion. In terms of the etching type and depth, the localized corrosion resistance of the interface followed the sequences of Interface-⬚ > Interface ⬚ > Interface-⬚ > Interface-I ~ Interface-⬚ >Interface-⬚. As the whole, the resistivity towards chemical etching of the interface was directly related to the interfacial bonding performance which was severely affected by the quality of substrate pretreatment. Interfacial corrosion of the laminated Ni structure, during selectively release process of ultra-thick sacrificial layer, led to a commensurate reduction in interfacial bonding strength and ultimately structural integrity.

In order to diagnose corrosion type and study corrosion mechanism, the evolution of corrosion damage were investigated. As indicated by the time sequence presented in Figure 6, pits (sub-micrometer scale) initiated along the interface at 30min and over time, grow to micro scale. Pits continually appeared and grow up and fuse with the neighboring one until a boundary trench formed on the whole interface. This was a kind of pitting corrosion which occurred only in microscopically thin zones along interface boundary.

Many authors had suggested that pit initiation was a consequence of the local breakthrough of the passive oxide film in the presence of the halogen ions, especially Cl^-, which had a smaller volume and better penetrating ability [30-31]. Interface-⬚where, because of dislocation and cavities in crystal structure, atoms were less thermodynamically stable than those at perfect lattice sites of base metal and passivating oxide film was thinner, had a greater tendency to corrode. Cl^- ions preferentially diffused or penetrate into the interface to react with metal to form the soluble compound. Successively, pits propagated in line with the defects distribution on the interface. These active pits were surrounded by the larger region of passive area. With the different potential between two regions, many passive-active microcells formed [32-33]. The anodic area was inside the pit ($Ni-2e^- \rightarrow Ni^{2+}$). And the cathodic zone was the external surrounding passive area, where oxygen (dissolved in the solution) and ferric reduction were

the main cathodic processes ($O_2 + 2H_2O + e^- \rightarrow 4OH^-$; $Fe^{3+} + e^- \rightarrow Fe^{2+}$). The initiatory grow-up rate of the pits was slow, only 0.12μm/min, calculated from the pit depth change from 30min to 70min. As exposure time going on, the circulation of microcell current gave rise to a series of reactions and chemical modifications: inside pit, pH decrease due to the hydrolysis of dissolved nickel cations ($Ni^{2+} + H_2O \rightarrow Ni(OH)_2 + 2H^+$) to further stimulate the anodic attack. As a result, the etching rate became as high as approximately 0.55μm/min which was calculated from the pit depth change from 70min to 90min. Further, pitting corrosion proceed inside the interface zone and spread on the surface. Simultaneously, the adjacent pits fused into each other. The pits fusion widen the pit mouth and quicken the ion exchange between pit inside and outside, resulting in the acidity decreasing. And the pit etching rate slowly dropped to 0.47μm/min from 90min to 120min, preventing the pits from spreading deeper. Consequently, wide and shallow boundary trench instead of narrow and deep cavity formed along the interface.

In conclusion, the pitting corrosion of the Ni/Ni interface in the process of releasing the ultra-thick Cu sacrificial layer comprises three main processes, pit initiation, pit growth and pits fusion. Pit initiation is the kinetic limiting step. The pit initiation time of the Interface-Ⅰis about 30min while that of the Interface-Ⅱ and Interface-Ⅲ are about 40min and 60min, respectively. For Interface-Ⅳ, the pit initiation time was as long as 100~120min. Dramatically, even selectively etching time last 140min, no visible pits appeared on Interface-Ⅴ. Pit initiation is closely related with the interfacial property. The more the interface defects are, the longer the pit initiation time is. Besides, pits fusion is also a crucial step, which has an important effect on the pit growth rate and corrosion shape. The detailed pitting corrosion mechanism of the Ni/Ni Interface from both front view and cutaway view was depicted in Figure 7.

For ultra-thick (>700μm) sacrificial layers, the releasing process is time-consuming, even as long as several days. To improve releasing rate and manufacturing efficiency, strong oxidizers are indispensable, which always contain haloid ions, e.g. hydrochloric acid, cupric chloride, or can decompose to produce haloid ions, e.g. chlorite, hypochlorite, periodate. Predictably, the analogous localized corrosion behavior of multi-layered Ni or NiFe microstructure will also appear in these etchants like in ferric chloride solution, severely decreasing the mechanical performance, reliability and longevity of the micro device. Proper substrate pretreatments and post-heat-treatment, which eliminate the connecting defects in the interface zone by the surface activation mechanism and thermally induced diffusion mechanism, can largely improve pitting-resistance property of the interface.

4. Conclusion

By adjusting the pre/post-treatments, six kinds of the Ni/Ni interfaces were papered and their corrosion behaviors in the process of releasing the ultra-thick (>700μm) Cu sacrificial layer were fully investigated. Because of the easy passivity of the Ni metal, neither degreasing nor anodic treatment could completely remove the impurities from the Ni substrate, which was revealed by XPS measurements, resulting in the imperfections on the Ni/Ni interface. Dipping in releasing etchants, which always contained aggressive ions, the Ni/Ni interface was more easily corroded than the base. And the pitting corrosion occurred in

microscopically thin zones along interface boundary. The corrosion mechanism was explored. It includes three main processes, pit initiation, pit growth and pits fusion. Pit initiation is the kinetic limiting step and controlled by the interfacial property. Pits fusion is another pivotal process which affects the pit growth rate and corrosion shape. Pickling pretreatment- heat post-treatment combined technique, ameliorating the interfacial property by the surface activation and thermally induced diffusion mechanism, has been shown to be effective in improving the pitting corrosion resistance of the Ni/Ni interface. Besides, adding anti-pitting inhibitor into etchants is another solution to avoid localized corrosion and will be investigated in future.

Declarations

Declaration of competing interest

The authors declare that we have no known competing interests or personal relationships that could have appeared to influence the work reported in this paper.

Data availability

The raw data required to reproduce these findings cannot be shared currently as the data also forms part of an ongoing study.

References

[1]J Sun, W Cheng, et al. Fabrication of Superhydrophobic Micro Post Array on Aluminum Substrates Using Mask Electrochemical Machining. Chinese Journal of Mechanical Engineering, 2018, 31: 72.

[2]J Sun, W Cheng, J L Song, et al. Fabrication of Microlens Array and Its Application: A Review. Chinese Journal of Mechanical Engineering, 2018, 31: 16.

[3] W L Shan, Y Yang, K T Hillie, et al. Role of oxide thickening in fatigue crack initiation in LIGA nickel MEMS thin films. Materials Science and Engineering: A, 2013, 561: 434-440.

[4]L Xu, Y Liu. A Microresonant Gas Sensor by Micro-Electroforming. Journal of Micro and Nano-Manufacturing, 2016, 4: 014501.

[5]M Zhao, L Du, C Du, et al. Liu, Quantitative study of mass transfer in megasonic microelectroforming based on mass transfer coefficient: Simulation and experimental validation. Electrochimica Acta, 2019, 297: 328-333.

[6] Z Zhao, L Du, Z Xu, L Shao. Effects of ultrasonic agitation on adhesion strength of micro electroforming Ni layer on Cu substrate. Ultrasonics Sonochemistry, 2016, 29: 1-10.

[7] Z Zhao, P Zhu, L Yang, et al. Effect of dislocation density on adhesion strength of electroforming Ni layer on Cu substrate. Journal of Adhesion Science and Technology, 2018, 33: 1-13.

[8] C Zhang, B Liu, B Yu, et al. J. Influence of surface pretreatment on phosphate conversion coating on AZ91 Mg alloy. Surface and Coatings Technology, 2019, 359: 414-425.

[9] L Shao, L Wang, L Du. Inflence of initial current density on bonding strength between Ni layer and Cu substrate in microelectroforming. Journal of Adhesion Science and Technology, 2016, 30: 2013-2023.

[10] Z Zhao, L Du, Y Tao, et al. Enhancing the adhesion strength of micro electroforming layer by ultrasonic agitation method and the application. Ultrasonics Sonochemistry, 2016, 33: 10-17.

[11] J Liu, D Zhang, B Sha, et al. Fabrication of a three-layer SU-8 mould with inverted T-shaped cavities based on a sacrificial photoresist layer technique. Biomedical Microdevices, 2014, 16: 655-660.

[12] S Arai, T Hasegawa, N Kaneko. Fabrication of three-dimensional Cu/Ni multilayered microstructure by wet process. Electrochimica Acta, 2004, 49: 945-950.

[13] X Huang, G Liu, X Ying, et al. Applications of thick Sacrificial-Layer of zinc in LIGA process. Microsystem Technologies, 2008, 14: 1257-1261.

[14] K H Lau, A Giridhar, H Sekar. Releasing high aspect ratio SU-8 microstructures using AZ photoresist as a sacrificial layer on metallized Si substrates. Microsystem Technologies, 2013, 19: 1863-1871.

[15] D L Steven, T S Daniel. In-situ fabrication of sacrificial layers in electrodeposited NiFe microstructures. Journal of Micromechanics and Microengineering, 1999, 9: 97-104.

[16] L Du, M Zhao, A Wang, et al. Fabrication of novel MEMS inertial switch with six layers on a metal substrate. Microsystem Technologies, 2015, 21: 2025-2032.

[dataset] [17] Y B Wu, G F Ding, H Wang, et al. Efficient solution to selective wet etching of ultra-thick copper sacrificial layer with high selective etching ratio. IEEE, 2011.

[18] G Zhang. EFAB: A novel, high-aspect-ratio true three-dimensional microfabrication process for rapid, low-cost desktop micromachining of MEMS. University of Southern California, Los Angeles, 1999, pp. 132-135.

[19]S Wen, X Ji, Y Zhou, et al. Corrosion behavior of the S136 mold steel fabricated by selective laser melting. Chinese Journal of Mechanical Engineering, 2018, 31: 108.

[20] M Li, A Seyeux, F Wiame, et al. Insights on the Al-Cu-Fe-Mn intermetallic particles induced pitting corrosion of Al-Cu-Li alloy. Corrosion Science, 2020, 176: 109040.

[21] I Moravcik, N S Peighambardoust, A Motallebzadeh, et al. Interstitial nitrogen enhances corrosion resistance of an equiatomic CoCrNi medium-entropy alloy in sulfuric acid solution. Materials Characterization, 2021, 172: 110869.

[22] R Viroulaud, J Swiatowska, A Seyeux,et al. Influence of surface pretreatments on the quality of trivalent chromium process coatings on aluminum alloy. Applied Surface Science, 2017, 423: 927-938.

[23] A Zarebidaki, H Mahmoudikohani, M R Aboutalebi. Microstructure and corrosion behavior of electrodeposited nano-crystalline nickel coating on AZ91 Mg alloy. Journal of Alloys and Compounds, 2014, 615: 825-830.

[24] L Wang, D Zhang, L Guo. Phase-segregated Pt-Ni chain-like nanohybrids with high electrocatalytic activity towards methanol oxidation reaction. Nanoscale, 2014, 6: 4635-4641.

[25] T Chen, H John, J Xu, et al. Influence of surface modifications on pitting corrosion behavior of nickel-base alloy 718. Part 1: Effect of machine hammer peening. Corrosion Science, 2013, 77: 230-245.

[26] M H Bina, F Dehghani, M Salimi. Effect of heat treatment on bonding interface in explosive welded copper/stainless steel. Materials and Design, 2013, 45: 504-509.

[27] H Yang, J Zou, Q Shi, et al. Analysis of the microstructural evolution and interface diffusion behavior of NiCoCrAlYTa coating in high temperature oxidation. Corrosion Science, 2019, 153: 162-169.

[28] T Massoud, V Maurice, L H Klein, et al. Intergranular effects on the local electronic properties of the passive film on nickel. Corrosion Science, 2013, 69: 245-251.

[29] E Sikora, D Macdonald. Nature of the passive film on nickel. Electrochimica Acta, 2003, 48: 69-77.

[30] U Angst, E Bernhard, C K Larsen, et al. Chloride induced reinforcement corrosion: Rate limiting step of early pitting corrosion. Electrochimica Acta, 2011, 56: 5877-5889.

[31] D Xiang, X D Cheng, C Q Yuan, et al. Structure of Micro-nano WC-10Co4Cr Coating and Cavitation Erosion Resistance in NaCl Solution. Chinese Journal of Mechanical Engineering, 2017, 30:1239-1247.

[32] J L Luo, M B Ives. Pit Propagation of Nickel and Nickel Molybdenum Alloys. Journal of The Electrochemical Society, 1997, 144: 3907-3913.

[33]J Soltis. Passivity breakdown, pit initiation and propagation of pits in metallic materials – Review. Corrosion Science, 2015, 90: 5-22.
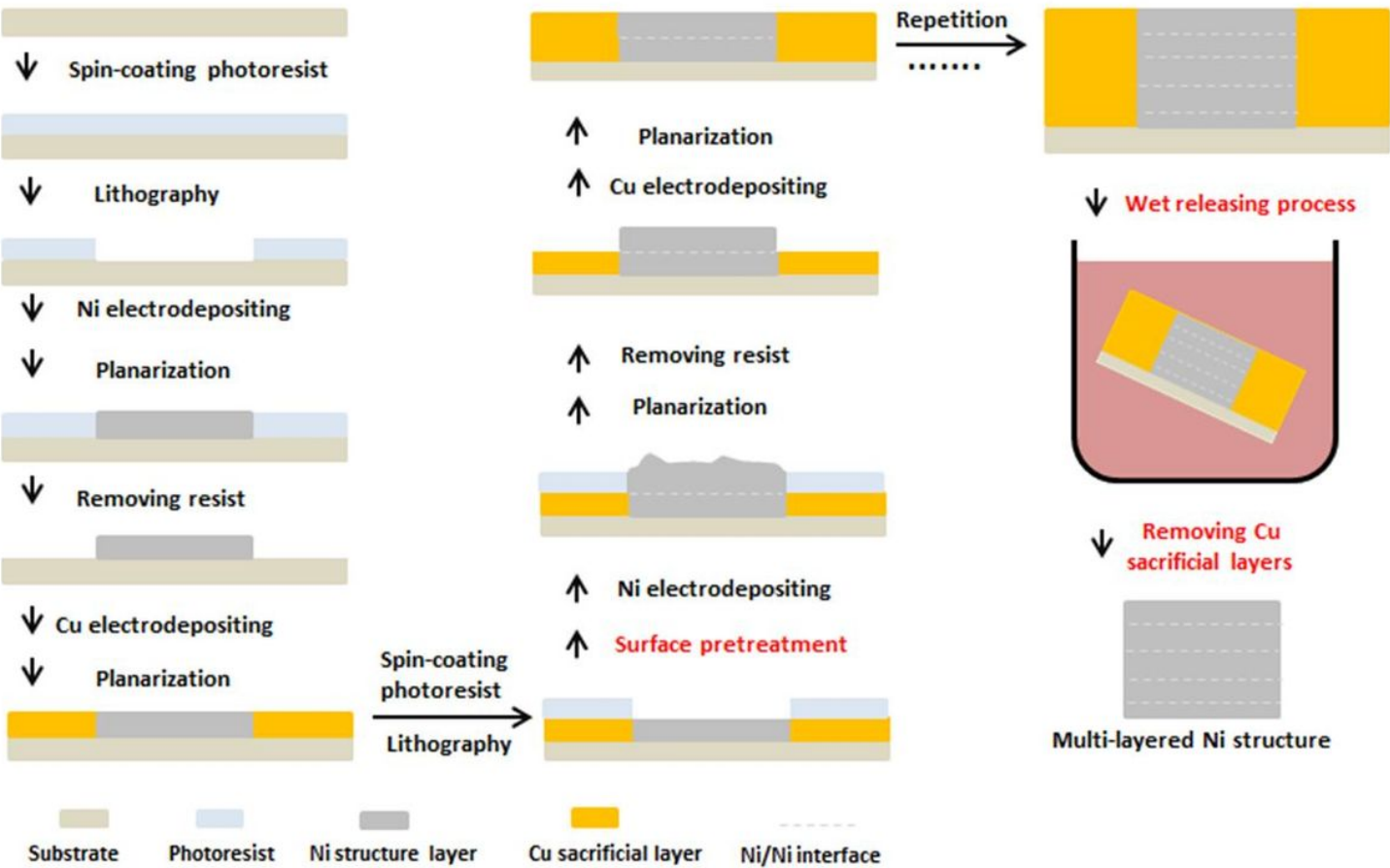
Figures

Figure 1

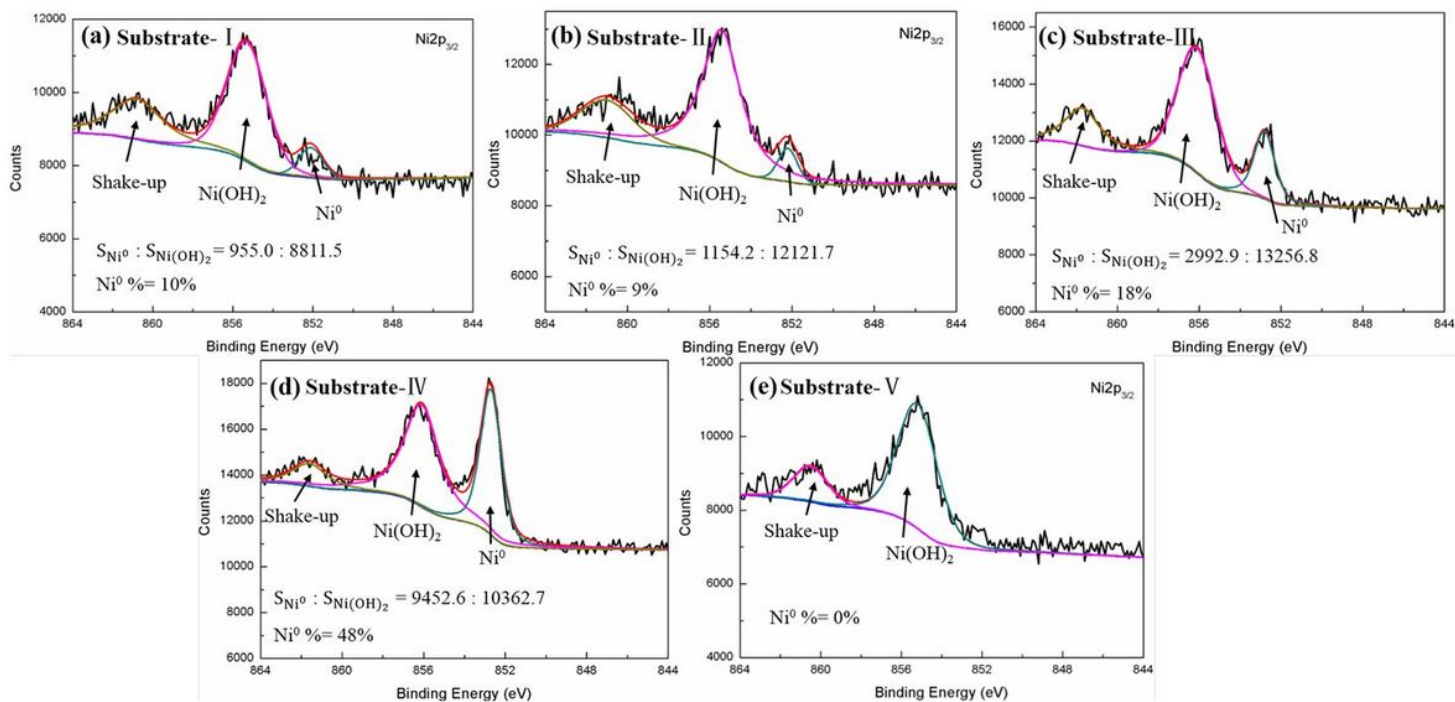Electroforming process of multilayer nickel structure

Figure 2

a) XPS Ni2p3/2 peaks of nickel substrates: (a)-(e) correspond to Substrate-Ⅰ, Substrate -Ⅱ, Substrate -Ⅲ, Substrate -Ⅳ and Substrate -Ⅴ respectively.
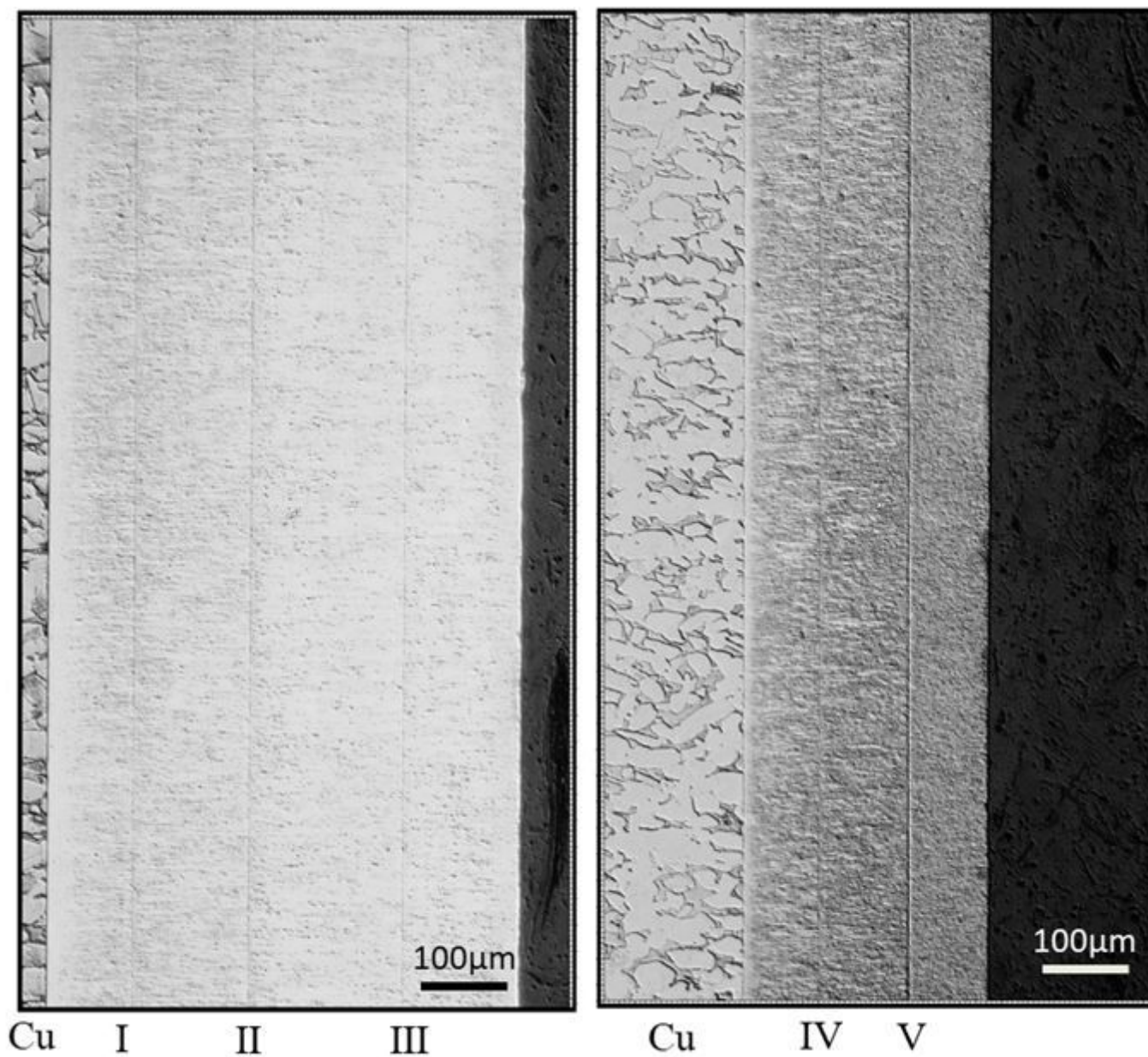
Figure 3

The cross-sectional metallography of the multilayered Ni structure observed by optical microscopy. The labeled Roman numerals, in sequence, refer to the Interface-Ⅰ, Interface-Ⅱ, Interface-Ⅲ, Interface-Ⅳ and Interface-Ⅴ.
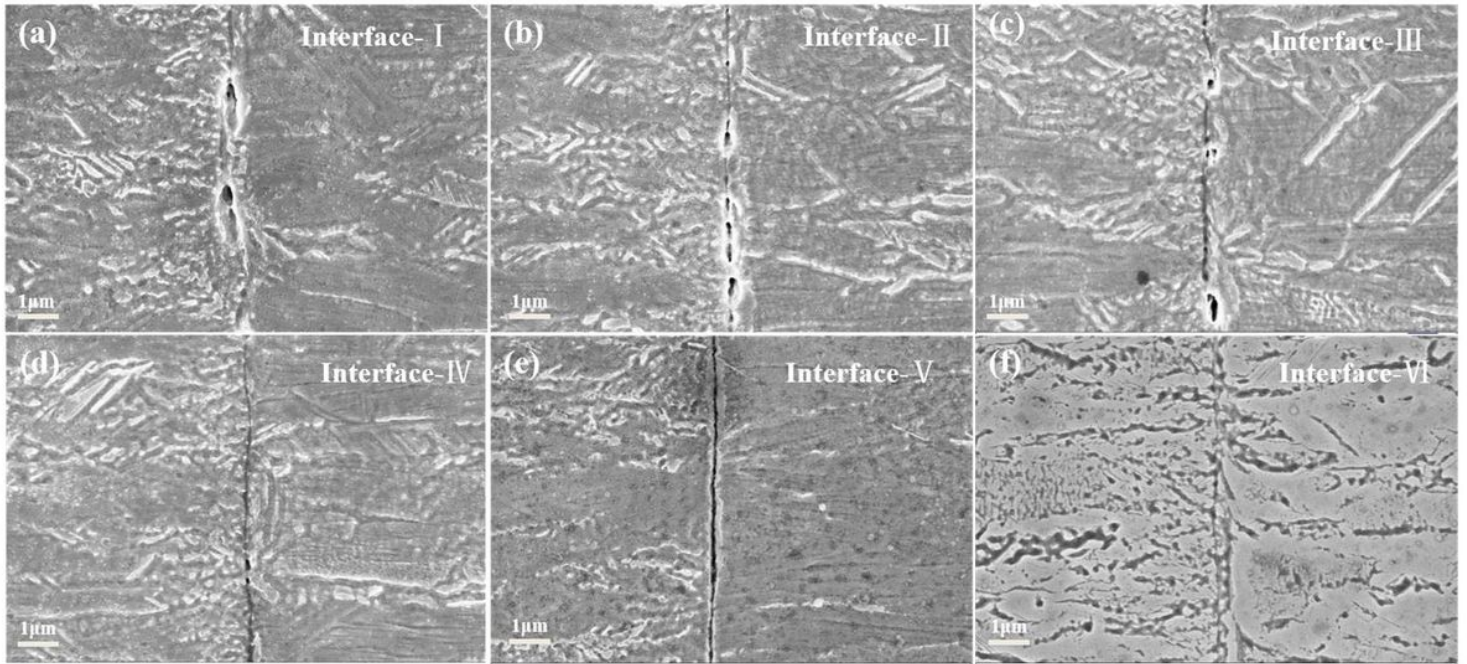
Figure 4

SEM images of the Ni/Ni interfacial morphologies etching in the metallographic etchant for three seconds; (a)-(f) were corresponding to the Interface-I, Interface-Ⅱ, Interface-Ⅲ, Interface-Ⅳ, Interface-Ⅴ and Interface-Ⅵ.

Figure 5

(a), (d) The etching images of the laminated Cu/Ni structures with ultra-thick Cu sacrificial layer in the ferric chloride solution for 120min; (b), (e) 3D view (top) and etching depth curve (bottom) of Cu/Ni interface; (c) 3D view (top) and etching depth curve (bottom) of Ni/Ni interface; (f) The amplified image recorded on the red framed region showing the detailed corrosion morphology of the Interface-Ⅳ; (g) The

corrosion image of the Interface-Ⅱ after etching for 140min; (h) 3D view (top) and etching depth curve (bottom) of Cu/Ni interface; (i) The enlarged image recorded on the green framed region.
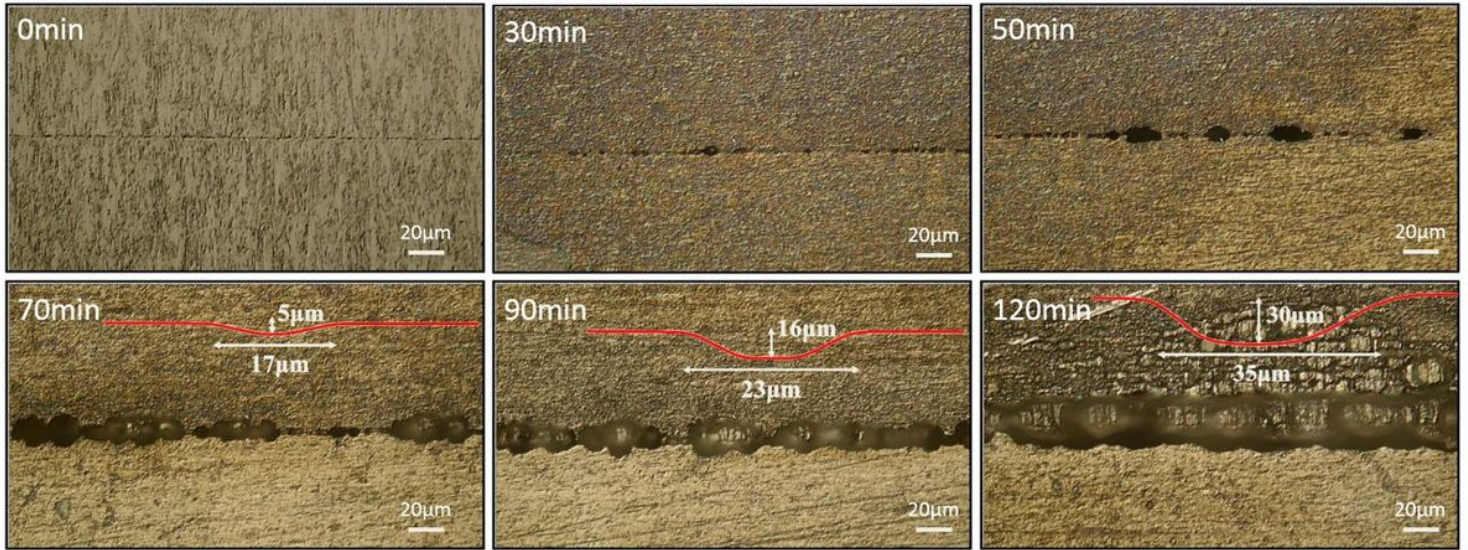

Figure 6

Evolution of corrosion damage on the Interface-Ⅱ at multiple immersion times. The insert curves were the cross-sectional contour lines of the pits, labeled by pit depth and diameter of pit mouth.
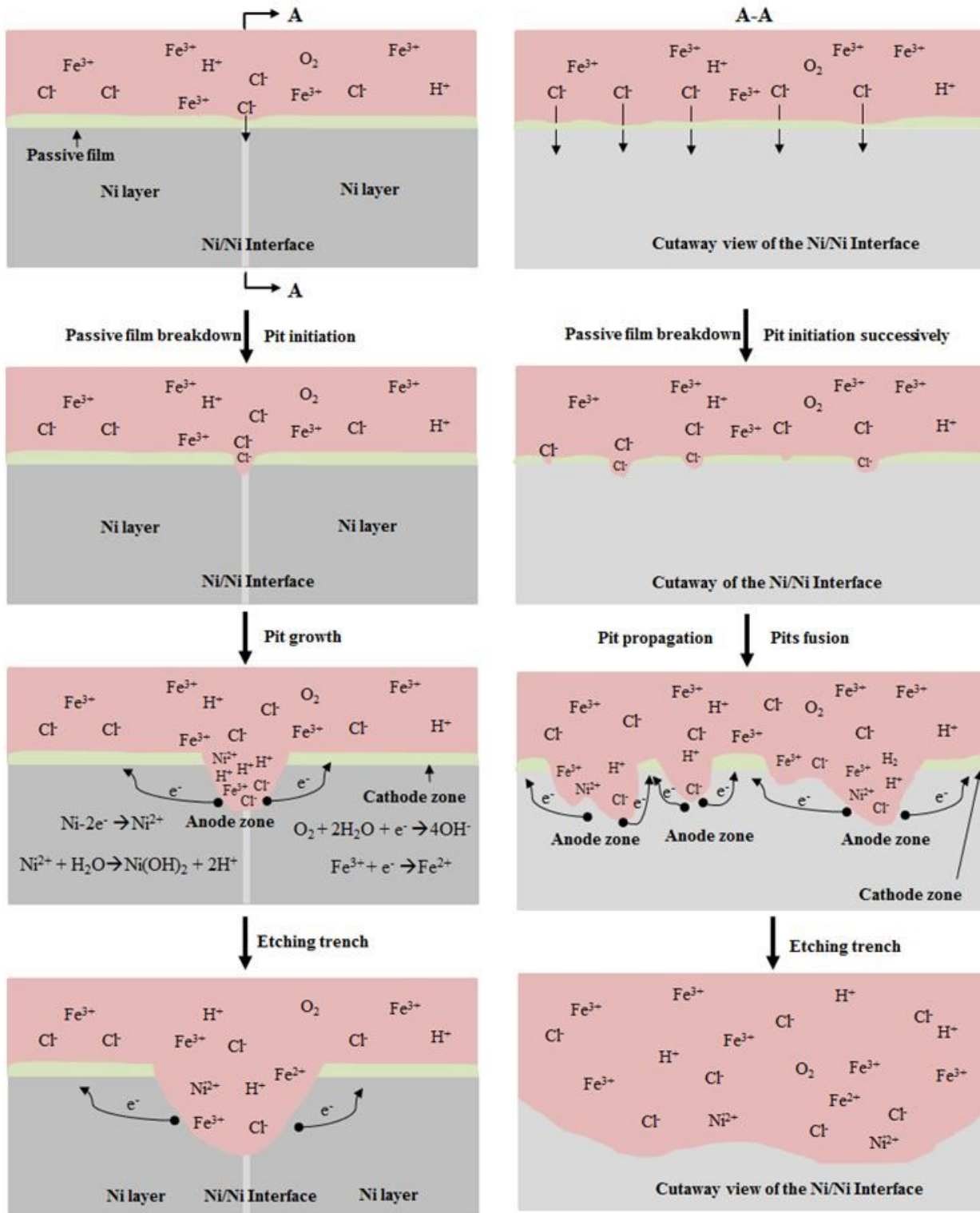
Figure 7

The schematic illustration of the pitting corrosion mechanism of the Ni/Ni Interface from front view (left) and cutaway view (right).